J. Webster (ed.), *Wiley Encyclopedia of Electrical and Electronics Engineering*

PROSTHETIC POWER SUPPLIES

Sensors and actuators operating inside the body to recuperate human organs have generated a great deal of interest during the last two decades (1,2,3,4,5). Advances in microelectronics have led to the development of powerful miniaturized devices, among them the various implantable artificial organs, sensors, and electrical stimulators (6,7,8,9,10,11). These devices have recently been intensively used in many disease circumstances, for example, cardiac pacemakers, cochlear implants, bladder controllers, bone growth stimulators, phrenic nerve stimulators, and functional neural systems, which are dedicated to lower-extremity and upper-extremity movements. Most of these advanced, commercially available devices are extracorporally powered through radio-frequency (*RF*) transmitting energy systems (12,13). All of them necessitate external, high-efficiency sources of energy. The majority of available prosthetic power supplies are based on amplitude modulation (*AM*) transmission, which rectifies a high-frequency signal (a carrier) to power on the implantable part.

Basic Principle of Prosthetic Power Supplies

Numerous alternatives are available for supplying power to implanted devices. The most important of these are the percutaneous plugs that break the skin to reach the implanted prosthesis. This connection may result in infection, risking implant damage and the safety of the patient. The second alternative is to use a battery (14). In this case, there are several disadvantages: frequent recharging or reimplantation is required and the battery occupies an important place relative to the device. The remaining alternatives are based on wireless techniques and they do not have any of the limitations mentioned previously. The goal of the transcutaneous energy transfer is to develop a safe and effective method for the remote delivery of energy to implanted biomedical devices, since this method draws power from an extracorporal source of energy and leaves the skin intact. These technologies allow patient mobility, improve quality of life, and reduce risk of infection. The transcutaneous links can be based on one of three categories of energy-transfer techniques: (1) electromagnetic, (2) optic (various forms of light), and (3) ultrasound. The electromagnetic radio-frequency inductively coupled link is the most commonly used technique to deliver power to prosthetics, and it is the most desirable method for patients. The inductively coupled power-transfer technique, however, lacks some characteristics such as high-energy-transfer efficiency and wide bandwidth, as well as transversal, orthogonal, and other inductance alignments.

In order to improve most of these limitations, other transdermal powering techniques have been proposed. In fact, a transcutaneous optical power converter has been introduced in Ref. 15. This method consists of solar cells receiving light from an external light source, which can be either a halogen-lamp- or a laser-diode-illuminated skin surface. Neither the optical nor the ultrasound transcutaneous power-supply techniques give the expected performances and they have been employed only in very restricted cases. The remainder of this article focuses on the characterization of the inductively coupled link, which remains the most appropriate choice because of its greater safety, efficiency and high tolerance to displacement. Thus, the external controller transmits power indefinitely at field levels that meet government safety standards (10 mW/cm^2) (8,12,16).

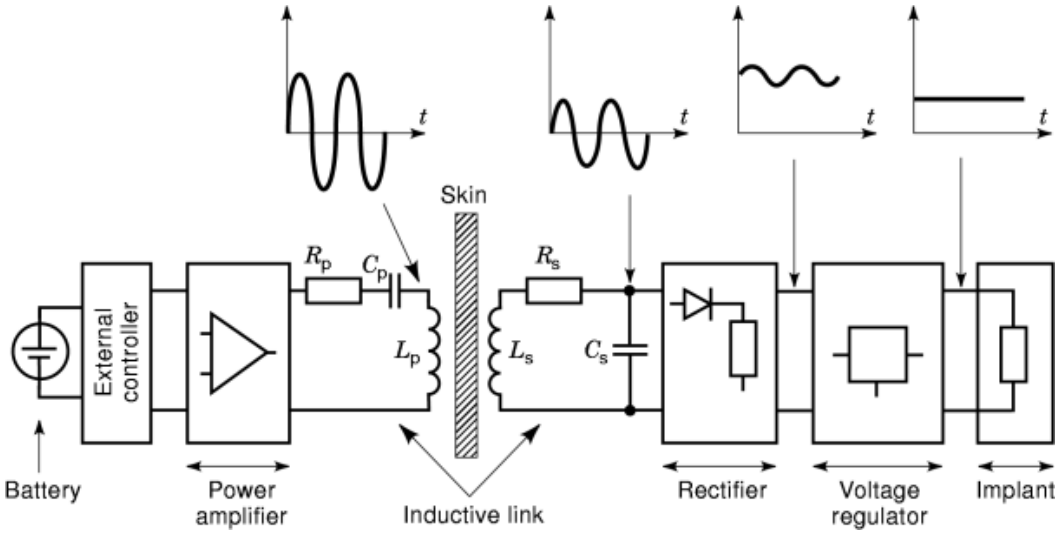

Fig. 1. Block diagram of a prosthetic device using an inductively coupled link. The purpose of the link is to transfer power and data to the implant.

Radio-Frequency Power Transfer Using an Inductively Coupled Link

A simplified generic block diagram of a system dedicated to power electronics implants using an inductive link is given in Fig. 1. The external part of such a system is driven by a power amplifier, which is the last stage of the RF transmitter. The implantable electronics device receives the necessary energy through this inductive link, which is followed by a rectifier and a voltage regulator. The voltage regulator delivers an adequate power supply and dc voltage to the electronics implant. The inductive link itself is composed of two series resonant circuits, a primary circuit (R_p, C_p, L_p) and a secondary circuit (R_s, C_s, L_s).

Analysis of the Inductively Coupled Link. In designing inductively coupled links to transfer energy to implantable devices, the most important characteristics to be considered are the ratio of the output voltage to the input voltage, the power efficiency, the bandwidth, the external power amplifier, and the load of the implant. The ac output voltage of the internal inductively coupled link should be high in order to allow the voltage regulator to extract the expected dc voltage as well as the energy to power on the whole implant device (Fig. 1). Based on the constraints mentioned earlier, the remaining sections of this article are devoted to determining the characteristics of the inductively coupled link. We begin by studying an unloaded inductively coupled link similar to that given in Fig. 2, and then we study the same link when the load and the amplifier output impedance are taken into account.

Ratio of the Output Voltage to the Input Voltage. The mesh equations of the unloaded inductively coupled link in Fig. 2 are the following:

$$V_{in} = Z_p I_p + j\omega M I_s \tag{1a}$$

$$0 = j\omega M I_p + Z_s I_s \tag{1b}$$

where

$$M = k\sqrt{L_p L_s} \tag{1c}$$

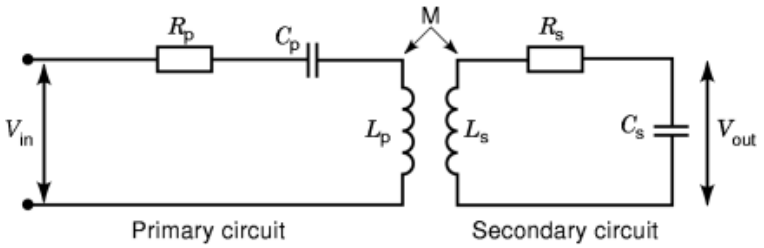

Fig. 2. Unloaded inductively coupled link.

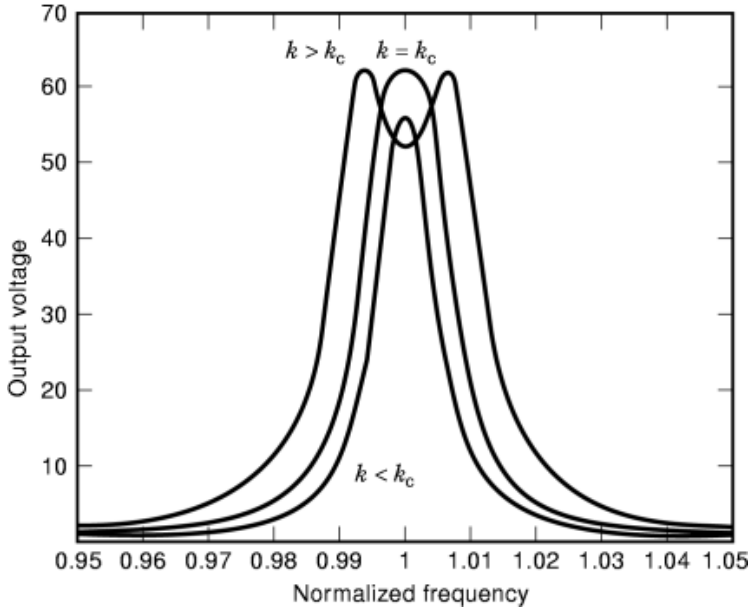

Fig. 3. Variation of the ratio (V_{out}/V_{in}) of the coupled link with frequency for different coefficients of coupling k for the case where the primary and secondary circuits are tuned to the same resonant frequency f_0.

is the mutual inductance between L_p and L_s, and k is the coefficient of coupling. Z_p and Z_s are the series impedances of the primary and secondary circuits, and they are given by

$$Z_p = R_p + j\left(\omega L_p - \frac{1}{\omega C_p}\right) \tag{2a}$$

$$Z_s = R_s + j\left(\omega L_s = \frac{1}{\omega C_s}\right) \tag{2b}$$

Since the coupled link is operated, in general, at the resonance frequency, let us assume that the primary (R_p, L_p, C_p) and the secondary (R_s, L_s, C_s) circuits are tuned to the same frequency f_0, so that

$$f_0 = \frac{1}{2\pi\sqrt{L_p C_p}} = \frac{1}{2\pi\sqrt{L_s C_s}} \tag{3}$$

By rearranging Eqs. (1a) and (1b), we can obtain the ratio of the voltage V_{out} developed across the capacitor C_s of the secondary circuit (V_{out}) to the input voltage applied in series with the primary circuit (V_{in}), as described in Ref. 17:

$$\frac{V_{out}}{V_{in}} = -\frac{1}{\gamma^2}\frac{k\sqrt{L_s/L_p}}{\left[k^2 + \frac{1}{Q_pQ_s} - h^2 + jh\left(\frac{1}{Q_p} + \frac{1}{Q_s}\right)\right]} \tag{4a}$$

$$\left|\frac{V_{out}}{V_{in}}\right| = -\frac{1}{\gamma^2}\frac{k\sqrt{L_s/L_p}}{\sqrt{\left(k^2 + \frac{1}{Q_pQ_s} - h^2\right)^2 + h^2\left(\frac{1}{Q_p} + \frac{1}{Q_s}\right)^2}} \tag{4b}$$

$$Q_p = \omega L_p/R_p = (2\pi f L_p)/R_p \tag{4c}$$

$$Q_s = \omega L_s/R_s = (2\pi f L_s)/R_s \tag{4d}$$

$$\gamma = f/f_0 \tag{4e}$$

$$h = 1 - \frac{1}{\gamma^2} \tag{4f}$$

where f is the operating frequency and Q_p and Q_s are the quality factors of L_p and L_s, respectively. The variation of $|V_{out}/V_{in}|$ with the frequency for different values of the coupling coefficient k is presented in Fig. 3. At the resonance frequency f_0, γ is equal to 1 and Eq. (4b) becomes

$$\left|\frac{V_{out}}{V_{in}}\right| = \frac{k\sqrt{L_s/L_p}}{k^2 + 1/(Q_pQ_s)} \tag{5}$$

Figure 4 shows the variation of the ratio $|V_{out}/V_{in}|$ as a function of k for a specific inductively coupled link. The maximum ratio is reached when the coefficient of coupling (k) is equal to the critical or optimal coupling k_c, which is given by

$$k_c = \frac{1}{\sqrt{Q_pQ_s}} \tag{6}$$

The ratio V_{out}/V_{in} is affected by the reflected impedance Z_{ref} from the secondary (receiving coil) circuit to the primary coil. This impedance is defined as follows:

$$Z_{ref} = (\omega M)^2/Z_s \tag{7}$$

The effect of this impedance on the primary circuit is exactly as if an impedance equal to $(\omega M)^2/Z_s$ had been added in series with the primary circuit. At resonance and at critical coupling, we have

$$Z_s = R_s \tag{8a}$$

(1)

and

$$k_c = \frac{1}{\sqrt{Q_p/Q_s}} = \frac{M}{\sqrt{L_p/L_s}} \tag{8b}$$

(2)

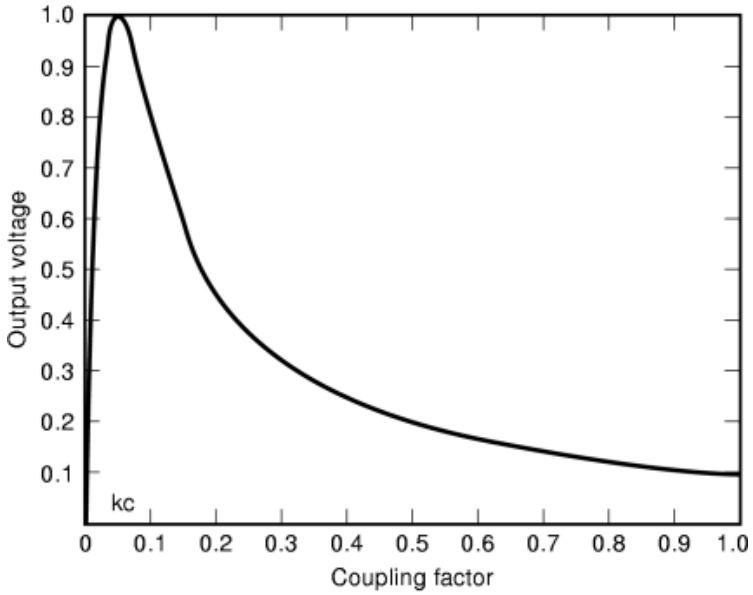

Fig. 4. Variation of the ratio (V_{out}/V_{in}) of the link with the coupling factor k at the resonance frequency f_0. The maximum of this ratio occurs at k equal to the critical coupling factor k_c.

The combination of Eq. (8b) with Eqs. (4b) and (4c) results in

$$\omega M = \sqrt{R_p/R_s} \qquad (8c) \tag{3}$$

then

$$Z_{ref} = (\omega M)^2/Z_s = R_p \Rightarrow Z_{ref} = R_p \qquad (8d) \tag{4}$$

Thus, the reflected impedance Z_{ref} is purely resistive and equal to the primary resistance R_p. With these conditions, the secondary current is maximal and the corresponding maximal possible voltage ratio V_{out}/V_{in} can be obtained from Eqs. (5) and (8b).

$$\left(\frac{V_{out}}{V_{in}}\right)_{max} = \frac{1}{2k_c}\sqrt{\frac{L_s}{L_p}} = \frac{1}{2}\sqrt{Q_p/Q_s}\sqrt{\frac{L_s}{L_p}} \qquad (9)$$

In this case, the corresponding dissipated power in the primary circuit can be calculated as follows:

$$P_{in} = \frac{V_{in}^2}{R_p + Z_{ref}} = \frac{V_{in}^2}{2R_p} \qquad (10)$$

Power Efficiency η_1. Based on the fact that the power delivered to the reflected impedance Z_{ref} is equivalent to the same quantity of power transferred to the secondary ($I^2{}_sZ_s$), the power efficiency η_1 of the

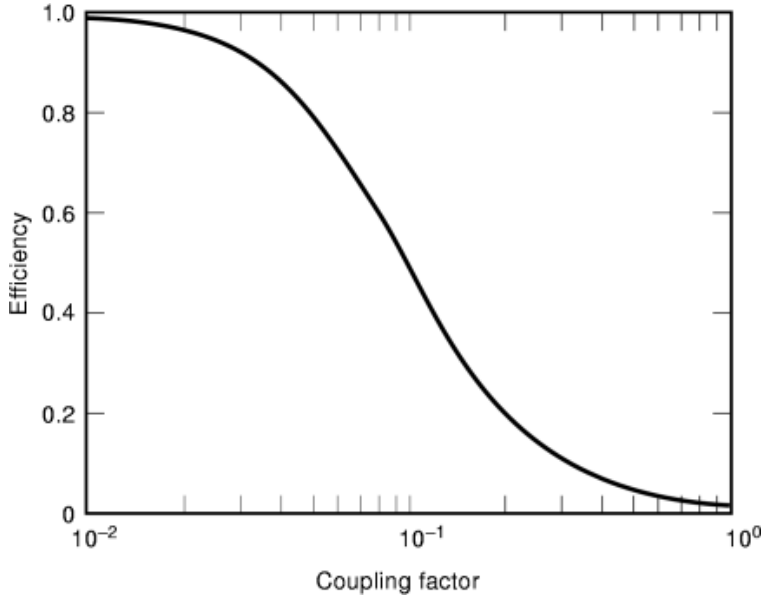

Fig. 5. Variation of power efficiency of the coupled link with the coupling factor k. The optimal value of this efficiency is equal to 0.5 which corresponds to the critical coupling factor k_c.

inductively coupled link can be expressed as (18,19)

$$\eta_l = \frac{Z_{ref}}{Z_p + Z_{ref}} = \frac{(\omega M)^2/Z_s}{Z_p + (\omega M)^2/Z_s} \tag{11}$$

At the resonance frequency f_0, Eq. (11) can be simplified to obtain

$$\eta_l = \frac{k_c^2}{k^2 + k_c^2} \tag{12}$$

The variation in the power efficiency η_l with the coupling coefficient k_c is depicted in Fig. 5. The optimum value of η_l is reached when both the secondary current I_s and the output voltage V_{out} are at their maximum values. This is possible only at the resonance frequency f_0 and at the critical coupling factor k_c. Then, from the Eq. (12), the optimal efficiency η_{lopt} is

$$\eta_{lopt} = \frac{k_c^2}{k_c^2 + k_c^2} = \frac{1}{2} \tag{13}$$

Thus, the optimal efficiency of an unloaded coupled link is equal to 50%, and this can be reached only at both the critical coupling factor and the resonance frequency.

Bandwidth of a Tuned Inductively Coupled Link at the Critical Coupling Factor. The bandwidth of a tuned inductively coupled link at the critical coupling coefficient and with identical quality factor coils (Q_p, Q_s) can be derived easily from the equations previously developed. In fact, at $k = k_c$ and $Q_p = Q_s = Q$, Eq. (4)

becomes

$$A = \left|\frac{V_{\text{out}}}{V_{\text{in}}}\right| = \frac{1}{\gamma^2}\frac{k_c\sqrt{L_s/L_p}}{\sqrt{(2k_c^2 - h^2)^2 + (2hk_c)^2}} = \frac{k_c\sqrt{L_s/L_p}}{\gamma^2\sqrt{4k_c^4 + h^4}} \tag{14}$$

At the resonance frequency f_0, and with $\gamma = 1$ and $h = 0$, Eq. (14) becomes

$$A_r = \frac{\sqrt{L_s/L_p}}{2k_c} \tag{15}$$

Equations (11) and (15) give

$$\frac{A}{A_r} = \frac{2k_c}{\gamma^2\sqrt{4k_c^4 + h^4}} = \frac{1}{\gamma^2\sqrt{1 + \frac{1}{4}(h/k_c)^4}} \tag{16}$$

Since the operating frequency of the inductive link is usually too close to the resonance frequency, and γ is so nearly unity between half-power points, thus to get $A/A_r = 1/\sqrt{2}$, the condition

$$h^2/2k_c^2 = 1 \quad \text{or} \quad \frac{h}{\sqrt{2}k_c} = 1 = \frac{f^2 - f_0^2}{\sqrt{2}f^2}Q \tag{17}$$

should be fulfilled. If we set $f = f_0 + \Delta f/2$, then Eq. (17) becomes

$$\frac{\Delta f/2(2f_0)(1 + \Delta f/4f_0)}{f_0^2(1 + \Delta f/2f_0)^2} = \frac{\sqrt{2}}{Q} \tag{18}$$

Generally $\Delta f/f_0 \ll 1$, so Eq. (18) can be simplified to lead to

$$\Delta f = \frac{f_0}{Q}\sqrt{2} \tag{19}$$

Inductive Link with the Amplifier and Load Impedances. If the effective resistance at the input of the regulator is R_{dc}, and with the assumption that the rectifier is ideal, then according to Ko, Liang, and Fung (18), the voltage peak value across C_s appears as a direct voltage across R_{dc} (Fig. 1). The equivalent ac load resistor R_{ac}, which dissipates an amount of ac power equivalent to the dc power in R_{dc} (16,18), is

$$R_{ac} = \frac{R_{dc}}{2} \tag{20}$$

Based on this assumption, a circuit equivalent to that in Fig. 1 can be obtained, as shown in Fig. 6(a). The resistor R_{ac} acts as a load to the inductively coupled link where the energy should be transferred. Now, if this

circuit is working near the resonance frequency and if R_{ac} is relatively high in comparison with R_s and ωL_s, then this circuit can be transformed to obtain the circuit in Fig. 6(b). Here R_L is the ac series resistor equivalent to the load resistance R_{ac} (18) and is equal to

$$R_L = \frac{(\omega L_s)^2}{R_{ac}} \tag{21}$$

The circuit in Fig. 6(b) is similar to that in Fig. 2, except that the series resistors of the primary and secondary circuits are affected by the presence of the output resistance of the power amplifier (R_g) and the resistance equivalent to the implant or load (R_{ac}). With these transformations, the equivalent series resistors (R_{ep}, R_{es}) and the quality factors (Q_{ep}, Q_{es}) of the primary and secondary circuits, respectively, are given by

$$R_{ep} = R_p + R_g \tag{22a}$$
$$R_{es} = R_s + R_L \tag{22b}$$

$$Q_{ep} = (\omega L_p)/R_{ep} \tag{23a}$$
$$Q_{es} = (\omega L_s)/R_{es} \tag{23b}$$

Replacing (Q_p, Q_s) in Eq. (5) by (Q_{ep}, Q_{es}), we obtain the new transfer function at resonance frequency V_{out}/V_{in}:

$$\frac{V_{out}}{V_{in}} = \frac{k\sqrt{L_s/L_p}}{k^2 + 1/(Q_{ep}Q_{es})} \tag{24}$$

The maximum of V_{out}/V_{in} occurs at the critical coupling $k = k_{ec}$, which is defined by

$$k_{ec} = \frac{1}{\sqrt{Q_{ep}Q_{es}}} \tag{25}$$

hence

$$\left(\frac{V_{out}}{V_{in}}\right)_{max} = \frac{1}{2k_{ec}}\sqrt{\frac{L_s}{L_p}} = \frac{1}{2}\sqrt{Q_{ep}Q_{es}}\sqrt{\frac{L_s}{L_p}} \tag{26}$$

The reflected impedance at resonance frequency is now given by

$$Z_{ref} = \frac{(\omega M)^2}{R_s + R_L} \tag{27}$$

Z_{ref} can be expressed in terms of R_{ac}, R_s, Q_p and Q_s, as (18)

$$Z_{ref} = \frac{R_{ac}k^2 Q_p Q_s}{R_s + Q_s^2 R_{ac}} R_p \tag{28}$$

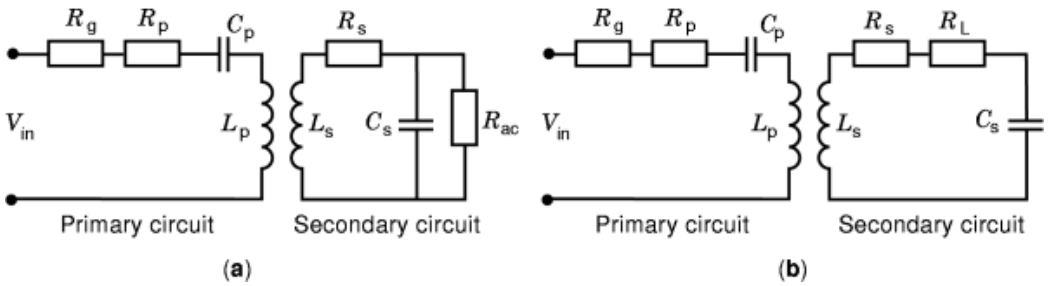

Fig. 6. Inductively coupled link: (a) with the amplifier and load resistances and (b) with the equivalent series resistor of the load.

and at $k = k_{ec}$, Z_{ref} becomes equal to R_{ep}, and at these conditions the power dissipated in the primary circuit is

$$P_{in} = \frac{V_{in}^2}{R_{ep} + Z_{ref}} = \frac{V_{in}}{2(R_g + R_p)} \tag{29}$$

The global power efficiency ($\eta = P_{out}/P_{in}$) can be determined by the power efficiency of the inductive link η_l and the efficiency of the secondary circuit η_s, where

$$\eta_l = \frac{Z_{ref}}{Z_p + Z_{ref}} = \frac{(\omega M)^2/Z_s}{Z_p + (\omega M)^2/Z_s} \tag{30}$$

and

$$\eta_s = \frac{R_L}{R_s + R_L} \tag{31}$$

$$\eta = \eta_l \eta_s = \frac{Z_{ref}}{Z_p + Z_{ref}} \frac{R_L}{R_s + R_L} \tag{32}$$

which could be expressed in term of R_{ac}, R_s, k, Q_p, and Q_s, as follows:

$$\eta = \frac{k^2 Q_p Q_s^3 R_s R_{ac}}{(R_{ac} + Q_p^2 R_s)[(1 + k^2 Q_p Q_s) R_{ac} + Q_s^2 R_{ac}]} \tag{33}$$

Coupling Coefficient and Mutual Inductance. The coupling coefficient k is related to the mutual M inductance by the relation $k = M/\sqrt{L_1 L_2}$, where L_1 and L_2 are the values of the primary and secondary inductances, respectively. Since the operating frequency of transcutaneous inductive links used to transfer power to prosthetics is in the radio-frequency range, the primary and secondary coils L_1 and L_2 have, in general, very small values. It follows that each of these coils is constructed of only one or a few small metal loops. For the general case, let us consider a system in which the primary and secondary coils are formed of one-turn circular loop each and are perfectly aligned (Fig. 7). The two coils are separated by the distance d and have r_1 and r_2 as radii.

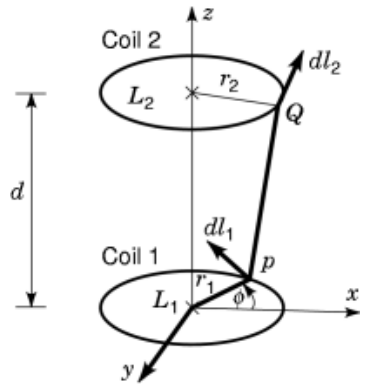

Fig. 7. Illustration of two perfectly aligned coils.

The general form of mutual inductance M between two coils of n_1 and n_2 turns is given by the following Neuman relationship (20):

$$M = \frac{\mu_0 n_1 n_2}{4\pi} \oint_{c_1} \oint_{c_2} \frac{dl_1 dl_2}{r_{12}} \tag{34}$$

Using this relation, the mutual inductance M of the system in Fig. 7 is

$$M = \mu_0 \sqrt{r_1 r_2} \left[\left(\frac{2}{f} - f \right) K(f) - \frac{2}{f} E(f) \right] \tag{35}$$

where μ_0 is the permeability of free space in henrys per meter and f is a variable defined by

$$f = 2\sqrt{\frac{r_1 r_2}{(r_1 + r_2)^2 + d^2}} \tag{36}$$

and $K(f)$ and $E(f)$ are the complete elliptic integrals of the first and second kind (20), respectively, defined as

$$K(f) = \int_0^{\pi/2} \frac{d\theta}{\sqrt{1 - f^2 \sin\theta}} \tag{37}$$

$$E(f) = \int_0^{\pi/2} \sqrt{1 - f^2 \sin^2\theta}\, d\theta \tag{38}$$

The values of L_1 and L_2 can be derived from Eq. (34), and are given by

$$L_i = L_i \mu_0 n_i^2 r_1 \left(\ln \frac{8r_i}{e_i} - 2 \right) \qquad e_i \ll r_i \quad \text{and} \quad i = 1, 2 \tag{39}$$

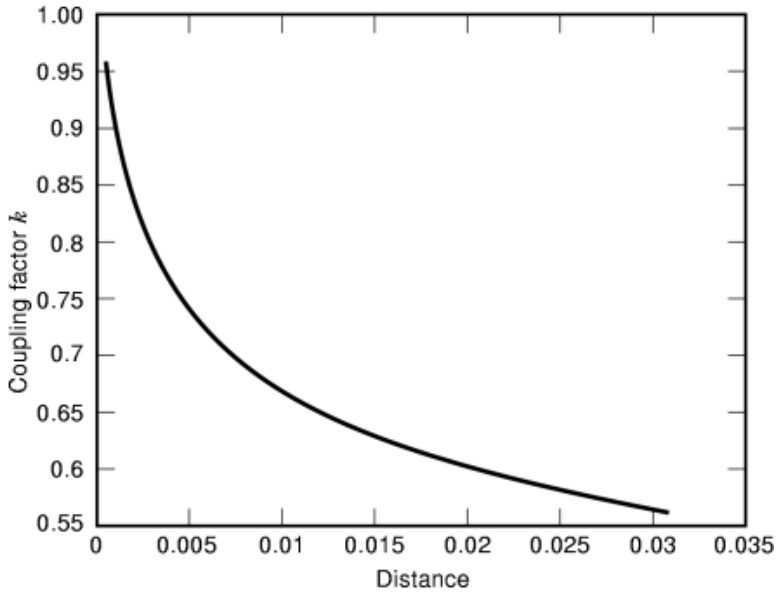

Fig. 8. Variation of the coupling coefficient k with the coil separation. The coupling factor is high when the separation of the two coils is small and decreases as this separation increases.

Here e_i is the wire radius of the coils. Using Eqs. (1) and (5), the variation of the coupling coefficient k as a function of coil separation d is shown in Fig. 8. The coupling coefficient is almost equal to 1 when the coil separation d is too small, but decreases rapidly as the separation d increases.

When the primary and secondary coils present a lateral or an angular misalignment, the calculation of the mutual inductance is complex and there is no single and precise formula for M for these cases. A good discussion and approximation formulas for the mutual inductance, for the case of the presence of the different misalignments, can be found in 21 and 22.

When the primary and secondary coils are constructed of more than one turn, a better arrangement of the coil loops described in Refs. 23 and 24 is preferred in order to enhance the coupling coefficient. In this arrangement, spiral coils are used in such a way that the turns are not concentrated at the circumferences, but distributed across the diameter. And, in order to reduce the magnetic flux leakage in the body, a set of amorphous fibers is attached radially on these spiral coils (23). These amorphous fibers increase the coupling coefficient and the inductance, which in turn reduces the magnetic flux leakage.

Power Amplifiers. The inductive link dedicated to transferring power to prosthesis necessitates the employment of a high-efficiency power amplifier. This helps to transfer the energy required by the implant with minimum loss in the side of the transmitter. The drives most used in the transmitter of a system using an inductive link are either class D or class E amplifiers. The reason behind the choice of these classes of amplifiers is their switching mode in operation, which provides them with high power efficiency.

The Class D Power Amplifier. An example of a class D amplifier is shown in Fig. 9. It uses a pair of power metal oxide semiconductor (*MOS*) transistors followed by a series resonant circuit (the primary circuit of the inductive link). Each transistor acts as a low-loss switch, which has only two states: the ON state (conducting) and the OFF state (nonconducting). The two transistors are alternately opened and closed at very high speed, resulting in a rectangular voltage waveform at the output of the amplifier. In its ON state, the MOS transistor acts as a small resistor; therefore the power loss is very small; in its OFF state, the leakage current is very small and again the power loss is negligible. When the resonant circuit is tuned to the

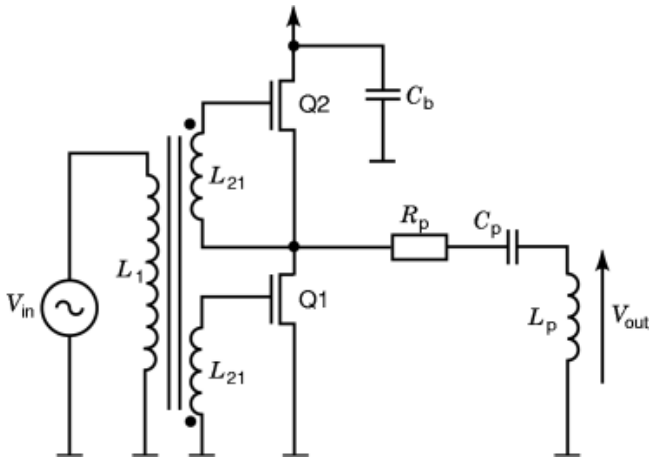

Fig. 9. Class D power amplifier based on a two MOS transistors (switches). The switch mode operation of these transistors helps to reduce the power loss of the amplifier. The amplifier works efficiently when operated at a frequency equal to the resonant frequency f_0 of the inductively coupled link.

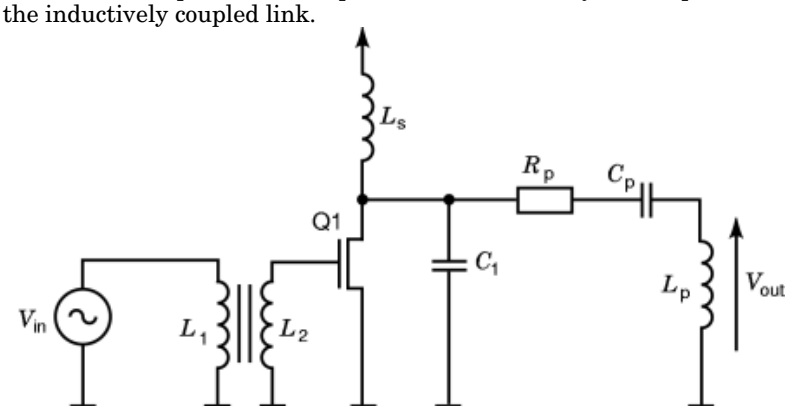

Fig. 10. Class E power amplifier based on a single MOS transistor acting as a switch. As in the case of the class D amplifier, the switching mode operation of the transistor makes this kind of amplifier provide a very high power efficiency.

switching frequency of the transistors, it presents low reactance to the fundamental and high reactance to all the harmonics. It follows that the output voltage V_{out} is a sinusoidal waveform with a frequency equal to the switching frequency of the transistors. Due to the low power loss in the transistors, the class D power amplifier in general offers very high efficiency (>90%), which depends on the switching characteristics of the transistors. If the switching time of the transistors is very small, then the class D amplifier can provide good performances at the frequency range of the inductive link. Due to these interesting characteristics, researchers have proposed many approaches (12,13,16) based on the class D amplifier to power various biomedical prosthetics.

The Class E Power Amplifier. The class E amplifier uses only one power transistor followed by a series resonant circuit (the primary circuit of the inductive link) (Fig. 10). The power transistor acts, in this case, as a low-loss switch. This will keep the amplifier's power loss at a very low level. The primary circuit of the coupled coils and the capacitor C_1 are tuned to a frequency close to the switching frequency of the transistor. This will result in a sinusoidal waveform at the output. The power efficiency of the class E amplifier can theoretically reach 100%. The class E power amplifier is used in many designs (5,25,26) to transfer power to prosthetic implants.

Main Inductively Coupled Link Approaches

The desired high performances of transcutaneously powered devices are subject to parameter variations such as inductively coupled link misalignment, distance variations between emitter and receiver coils, operating frequency drift, and the change in electronic component values. But ideally, link performances such as the voltage gain and the power efficiency have to be insensitive to any of these changes. A great deal of interesting theoretical and experimental research has already been done in the field of the design of inductively coupled links dedicated to transferring power and data to prosthetic implants (12,13,16,18,19,21,26,27,28). Few of these available designs dealt with techniques for reducing the effect of variations of link parameters on its performances, however. Usually, these techniques focused primarily on the optimization of transcutaneous link performances, and secondly on minimizing the effect of link characteristic variations. The following sections describe briefly the main existing approaches that deal with inductively coupled link effect variations.

The Geometric Approach. Galbreith, Soma, and White (12) proposed a common approach, called the geometric approach, which is used to reduce the effects of coupling variations. In this approach, the receiver and transmitter coils are of different sizes, with the receiver coil being the smaller one. In this way, the coupling factor is insensitive to the coil displacement, assuming that the receiver coil remains within the perimeter of the transmitter coil. The coils are allowed to move laterally, and even with small angular rotations, without significant changes in k. This interesting characteristic makes this approach tolerant to the various misalignments, but still sensitive to coil separation changes. The authors of this approach explain that for small separations, the coupling coefficient drops in proportion to the coil separation (12). And, since the voltage gain of the link is dependent on the coupling coefficient, this approach is not tolerant to the coil separation. Another problem with this approach arises from the fact that the transmitter and receiver coils are not of equal size. In this case, the coupling magnitude is smaller than that resulting from coils of equal size. With this reduction in the coupling magnitude, the current magnitude of the transmitter coil has to be high to obtain the same voltage gain as in the case of equally sized coils. But increasing the transmitter's current leads to significant losses in the primary loop, which has to be avoided.

The Stagger-Tuning Approach. Another approach that desensitizes the voltage gain of the inductive link to the coupling was also proposed in Ref. 12. This approach offers good displacement tolerance, efficiency, and large bandwidth. In this approach, the inductively coupled link is based on the stagger-tuning principle where both the receiver and the transmitter resonant frequencies are not equal and they are slightly different from the link operating frequency. The poles associated with these two frequencies are selected so that one pole is placed above the pole associated with the operating frequency and the other pole below. The position of these poles, however, is subject to the coupling changes. The key to this stagger-tuning approach is to place these poles in such a way that their movement will compensate for the link gain resulting from the coupling changes. For example, an increase in the coupling will normally result in an increase in the link gain, but at the same time the poles will move away from the pole associated with the operating frequency, which normally decreases the gain. These opposite effects cancel each other out and force the link gain to be insensitive to the coupling variations caused by the coil displacement. Therefore, the stagger-tuning approach is not only tolerant to the angular and lateral misalignment, but also to coil separation. Also, this pole placement increases the link bandwidth without affecting the link voltage gain and power efficiency.

Another Approach. Another interesting design approach which is insensitive to coupling variations was proposed by Zierhofer and Hochmair (29). This approach focuses on optimization of the link power efficiency and coil misalignment tolerance. In this approach, a high-efficiency self-oscillating class E power amplifier is used to drive the transmitter-tuned circuit. The key to this design is that the amplifier oscillating frequency is not fixed, but affected by the coil coupling variations. The effect of coupling variations due to coil distance changes results in the changing of the reflected impedance of the receiver in the transmitter-tuned circuit. The variation in the reflected impedance is then used to control the oscillating power amplifier frequency. Zierhofer

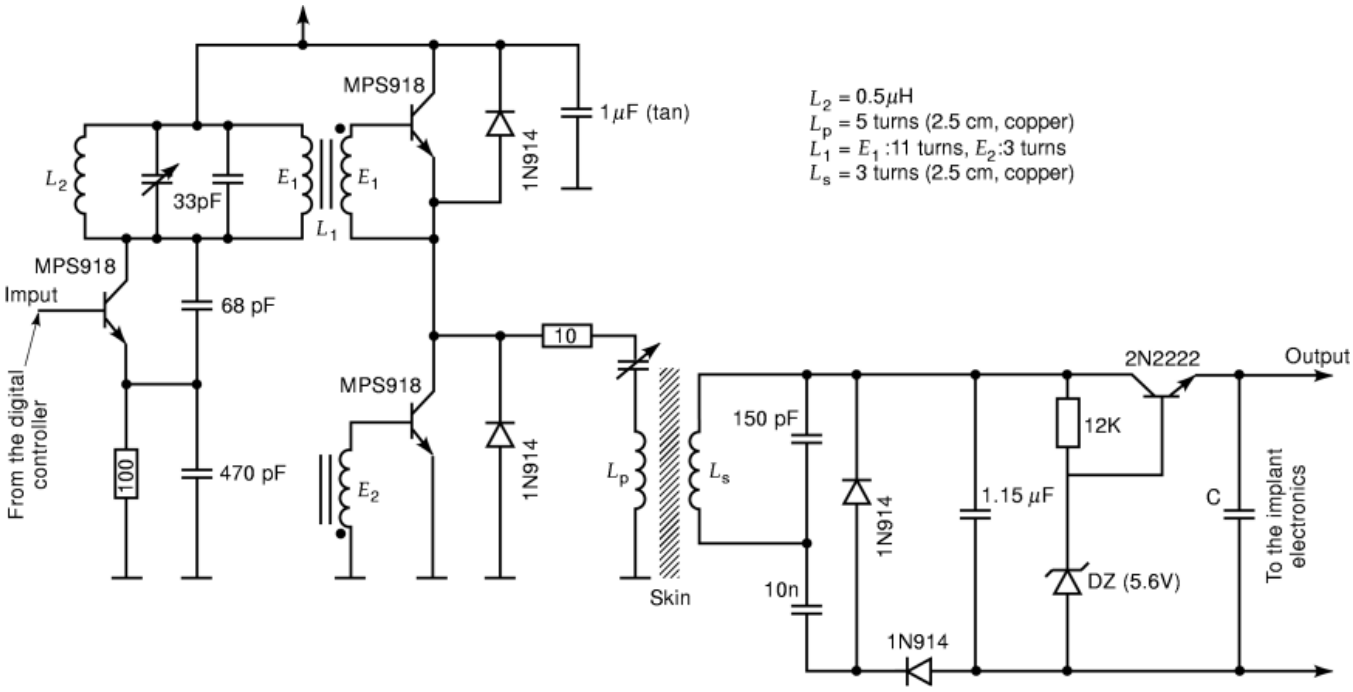

Fig. 11. The inductive coupling stage circuit. The main blocks of this circuit are a class D power amplifier driven by an oscillator, a series inductively coupled link, and a voltage regulator.

and Hochmair have shown that the amplifier oscillating frequency tracks the absolute transmission efficiency maximum, thereby improving the power transmission against the coupling variation. Since the coupling is dependent on coil separation, this approach is tolerant to the coil distance variations.

An Example of Applications. Figure 11 depicts an example of the schematic of a complete transmission energy and data circuit. It encloses a 20 MHz AM modulator that produces a carrier, the amplitude of which is modulated by the incoming Manchester-coded data (8). The resulting modulated carrier is then presented to a class D amplifier, the output of which is controlled by a power regulator. This device is intended to compensate for the variations in the coupling factor affected by the displacements between the transmitting and receiving coils. It increases the power voltage of the class D amplifier in the case of a high coupling and it reduces the power voltage in the reverse case (13). The secondary output signal of the transformer is then presented to a voltage regulator and an AM demodulator to provide coded data and power to the whole implant. By using such a system, two main objectives are sought: a minimum transmission bandwidth of about 1 MHz, since it has been designed for a maximum transmission rate of 500 kbit/s, and minimal losses to ensure the external power source durability of the future miniaturized system. To reach these two objectives, we have opted for a stagger-tuned link (12). Together with the power regulator technique, the link features low-energy consumption and possesses the advantage of a wide bandwidth (13) in addition to its adaptability to coil displacement. It also produces a fairly stable output voltage from which to recuperate a regulated voltage supply. The voltage regulator used in our system operates with a small voltage drop across it, so that it consumes little power while sourcing large currents, thus respecting the second consideration mentioned above. In the same vein, we note that the choice of the 20 MHz carrier depends on transformer efficiency, since a computer simulation model and experimental tests (Fig. 12) have indicated a maximum efficiency (24%) at this frequency.

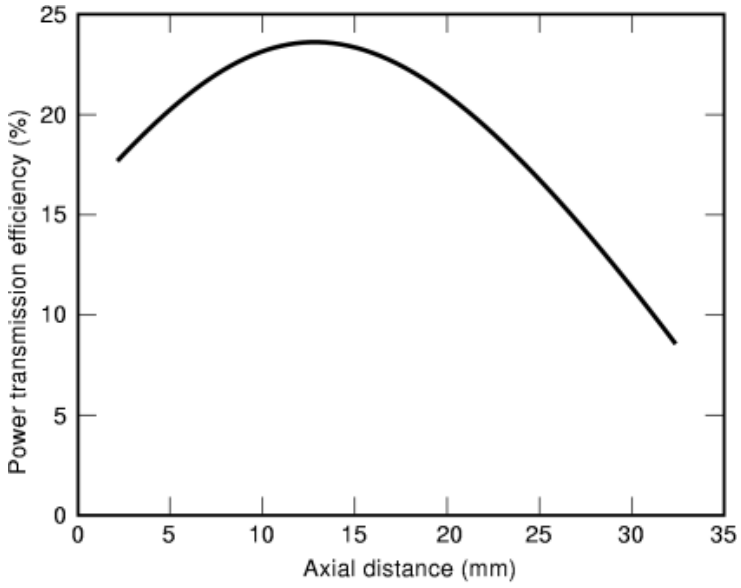

Fig. 12. Variation of the power efficiency with the coil separation of the circuit presented in Fig. 11. The efficiency maximum is equal to 24% and is obtained at a frequency equal to 20 MHz and at the critical coupling of the inductively coupled link.

Summary and Future Developments

With the recent developments in the microelectronics field, new complex and powerful implants with small sizes can be now achieved with minimum cost and in a short time. Unfortunately, we still have to overcome the critical problem of powering these implants. Therefore, there is an immediate need to develop new, small-sized powering systems with high efficiency. Since these implants are, in general, intended for long-term implantation periods, the use of batteries is to be avoided whenever it is possible. By avoiding the use of batteries to power implants, the surgery needed to replace the implant batteries becomes unnecessary, which will in turn reduce the risk of skin infection. From the present article, it is obvious that a powering system based upon an inductively coupled link presents a good choise for such applications. With this choice, the implant lifetime is no longer limited by the powering system lifetime, but only by the implant electronics. Since, with the use of an inductively coupled link, the energy transfer is achieved electromagnetically, the skin damage risk is kept to a very low level. The other interesting characteristic of the inductively coupled link is that it can be used to accomplish the dual tasks of bidirectional communication and energy transfer simultaneously. Currently, many researchers are developing new implants and new powering systems based on the class D and E power amplifiers and using inductively coupled links. The challenge is to integrate the implant electronics, the receiving power system, and the communication system in the same chip. In some cases, new storage elements are also to be included within the same chip to make the implant autonomous. The amount of energy transferred should be high enough in order to power the electronics of the whole implant. Finally, the powering system should a high-efficiency one so that the whole system remains economical.

BIBLIOGRAPHY

1. W. F. Agnew D. B. McCreery *Neural Prostheses, Fundamental Studies*, Englewood Cliffs, NJ: Prentice Hall, 1990.
2. W. Greatbatch C. F. Holmes History of implantable devices, *IEEE Eng. Med. Biol. Mag.*, **10** (3): 38–41, 1991.
3. L. J. Seligman Physiological simulators: From electric fish to programmable implants, *IEEE Trans. Biomed. Eng.*, **29**: 270–284, 1982.
4. M. C. Shults *et al.* A telemetry-instrumentation system for monitoring multiple subcutaneously implanted glucose sensors, *IEEE Trans. Biomed. Eng.*, **41**: 937–942, 1994.
5. D. F. Williams Implantable prostheses, *Phys. Med. Biol.*, **25**: 611–636, 1980.
6. E. Feigenbaum Cochlear implant devices for the profoundly hearing impaired, *IEEE Eng. Med. Biol. Mag.*, **6** (2): 10–21, 1987.
7. J. T. Mortimer Electrical excitability: The basis for applied neural control, *IEEE Eng. Med. Biol. Mag.*, **2** (2): 12–13, 1983.
8. M. Sawan *et al.* Stimulator design, and subsequent stimulation parameter optimization for controlling micturition and reduction urethral resistance, *IEEE Trans. Rehabil. Eng.*, **4**: 39–46, 1996.
9. B. Smith P. H. Peckham M. W. Keith An externally powered multichannel implantable stimulator for versatile control of paralyzed muscle, *IEEE Trans. Biomed. Eng.*, **34**: 499–507, 1987.
10. R. B. Stein P. H. Peckham D. Popovic, (eds.) *Neural Prostheses: Replacing Motor Function after Disease or Disability*, Oxford: Oxford University Press, 1992.
11. M. Thoma *The Leg Pacemaker*, Vienna: MedImplant, Vienna, 1993, p. 4.
12. D. C. Galbraith M. Soma R. L. White A wide-band efficient inductive transdermal power and data link with coupling insensitive gain, *IEEE Trans. Biomed. Eng.*, **BME-34**: 265–275, 1987.
13. M. Sawan *et al.* A new transcutaneous fully-programmable neural stimulator, *Int. J. Microcomput. Appl.*, **13**: 142–147, 1994.
14. D. C. Jeutter A transcutaneous implanted battery recharging and biotelemeter power switching system, *IEEE Trans. Biomed. Eng.*, **BME-29**: 314–321 1982.
15. T. Tamura *et al.* Transcutaneous optical power converter for implantable devices, *Proc. SPIE*, **2084**: 99–104, 1996.
16. N. De N. Donaldson T. A. Perkins Analysis of resonant coupled coils in design of radio frequency transcutaneous links, *Med. Biol. Eng. Comput.*, **21**: 612–627, 1983.
17. F. E. Terman *Radio Engineering Handbook*, New York: McGraw-Hill, 1943.
18. W. H. Ko S. P. Liang C. D. F. Fung Design of radio-frequency powered coils for implant instruments, *Med. Biol. Eng. Comput.*, **15**: 634–640, 1977.
19. Z. Tang *et al.* Data transmission from an implantable biotelemeter by load-shift keying using circuit configuration modulator, *IEEE Trans. Biomed. Eng.*, **42**: 524–528, 1995.
20. C. T. A. Johnk *Engineering Electromagnetic Fields and Waves*, New York: John Wiley & Sons, 1988.
21. E. S. Hochmair System optimization for improved accuracy in transcutaneous signal and power transmission, *IEEE Trans. Biomed. Eng.*, **BME-31**: 177–186, 1984.
22. M. Soma D. C. Galbraith R. L. White Radio-frequency coils in implantable devices: Misalignment analysis and design procedure, *IEEE Trans. Biomed. Eng.*, **BME-34**: 276–282, 1987.
23. H. Matsuki T. Matsuzaki A. Suzuki Energy transfer system utilizing amorphous wires for implantable medical devices, *IEEE Trans. Magn.*, **31**: 1276–1282, 1995.
24. C. M. Zierhofer E. S. Hochmair High-efficiency coupling-insensitive transcutaneous power and data transmission via an inductive link, *IEEE Trans. Biomed. Eng.*, **37**: 716–722, 1990.
25. Z. Hamici R. Itti J. Champier A high-efficiency power and data transmission system for biomedical implanted electronic devices, *Meas. Sci. Technol.*, **7**: 192–201, 1996.
26. P. R. Troyk M. A. K. Schwan Closed-loop class E transcutaneous power and data link for microimplants, *IEEE Trans. Biomed. Eng.*, **39**: 589–599, 1992.
27. I. C. Forster Preliminary development of a radiotelemetry system for biological applications, *Med. Biol. Eng. Comput.*, **24** (3): 281–291, 1986.

28. T. Mussivand *et al.* A Transcutaneous Energy and Information Transfer System for Implanted Medical Devices, 1996, *ASAIO Journal*, **41** (3): M253–M258.
29. C. M. Zierhofer E. S. Hochmair Geometric approach for coupling enhancement of magnetically coupled coils, *IEEE Trans. Biomed. Eng.*, **43**: 708–714, 1996.

ABDELOUAHAB DJEMOUAI
Ecole Polytechnique de Montréal
MOHAMAD SAWAN
Ecole Polytechnique de Montréal